A Unified Differential Mode Noise Estimation Method and Filter Size Comparison in Single-Phase Multileg and Multilevel Totem-Pole PFC Converters

Ali Tausif, *Student Member, IEEE*, and Serkan Dusmez, *Senior Member, IEEE*

***Abstract*—Wide-bandgap power devices have enabled single-phase totem-pole (TP) power factor correction (PFC) converter designs to be switched at several tens of kilohertz under hard-switching and hundreds of kilohertz under soft-switching. It is straightforward to analyze and compare the volume of boost inductor for TP PFC converters having multileg and multilevel configurations operating under continuous-conduction-mode (CCM) and critical-conduction-mode (CrM) at various switching frequencies; however, the impact of topology and switching frequency selections remains unchallenged for generated differential mode (DM) noise. This article proposes a unified and generalized DM noise estimation method for multileg, and multilevel TP PFC converters operated under both CCM and CrM operation modes. The method has been verified with simulation results obtained from various TP PFC topologies, as well as experimental results obtained from single-leg CCM and 4-Level CCM TP PFC converters. The empirically determined boxed sizes of DM filters have been compared among various TP PFC topologies, and the best switching frequency for each topology has been determined with the integration of boost inductor volume comparison.**

***Index Terms*—Differential-mode (DM) filter, DM noise, electromagnetic interference (EMI), interleaved, multilevel, power factor correction (PFC), switched-mode power supply, totem-pole (TP).**

I. Introduction

In order for power supply units (PSU) to be eligible for the industrial market, they must comply with certain electromagnetic interference (EMI) standards provided in IEC 61000-6-3 [1] and CISPR 25 [2]. With the introduction of wide-bandgap devices, particularly in emerging power electronics markets such as server/telecom and automotive industries, switching frequencies have been subjected to increase to achieve higher power densities [3], [4], [5] while EMI filter sizes still remain the same or get larger due to being not addressed well [6], [7], [8]. The unknown correlation between the switching frequency, power topology, and the EMI noise poses a great challenge for engineers to design compact and effective EMI filters.

When designing power supplies, especially continuous-conduction-mode (CCM) power factor correction (PFC) converters, a rule of thumb is to choose the switching frequency at 45, 67, and 135 kHz to limit the EMI noise appearing in the EMI spectrum, as the PFC inductor lowers the differential-mode (DM) noise by 20 dB per decade and several multiples of switching frequency harmonics remain below the 150-kHz limit. However, very little is known about multileg and multilevel CCM, and multileg critical-conduction-mode (CrM) totem-pole (TP) PFC converters.

In the majority of the design approaches and analyses, the volume of the boost inductor is considered independent of the DM filter design, where it is typically designed by defining a maximum inductor current ripple limit to be a predefined percentage of the peak input current, i.e., around 20%–25%. However, the boost inductor design cannot be isolated from the DM filter design, as the inductance helps lower the DM noise on top of its other benefits such as providing controllability and improving the total harmonic distortion (THD). Therefore, the switching frequency-inductance combination that provides the minimum total DM filter and boost inductor volumes should be chosen in high power-density designs. This necessitates evaluating DM noise and filter design models while designing the boost inductor of any PFC converter.

Many research efforts have been put into estimating the DM noise of conventional boost PFC topologies [9], [10], [11], [12], [13], [14]. In [13] and [14], DM noise estimation is analyzed for single-leg and two-leg interleaved topologies under a limited frequency range of 9–150 kHz. On the other hand, the works [15] and [16] cover both frequency bands, i.e., 9–150 kHz and 150–30 MHz for two-leg interleaved CCM boost PFCs. In [9], a generalized DM noise estimation approach is proposed; however, the impedance modeling of the converter needs to be obtained with the help of experimental data, and the necessity to solve a set of linear equations prolongs the process. The

Manuscript received 28 November 2022; revised 17 February 2023; accepted 6 March 2023. Date of publication 13 March 2023; date of current version 20 April 2023. This work was supported in part by European Union's Horizon 2020 Research and Innovation Programme under the Marie Sklodowska-Curie under Grant 101031029 and in part by the 2232 International Fellowship for Outstanding Researchers Program of TUBITAK under Grant 118C374. Recommended for publication by Associate Editor M. Hartmann. *(Corresponding authors: Serkan Dusmez; Ali Tausif.)*

Ali Tausif is with the Department of Electrical Engineering, Yildiz Technical University (YTU), 34349 Istanbul, Turkey (e-mail: ali.tausif@std.yildiz.edu.tr).

Serkan Dusmez is with the Power Management Solutions Department, WAT Motor Sanayi, 34349 Istanbul, Turkey (e-mail: serkan.dusmez@wat.com.tr).

Color versions of one or more figures in this article are available at https://doi.org/10.1109/TPEL.2023.3255543.

Digital Object Identifier 10.1109/TPEL.2023.3255543

DM noise estimation methods presented in [10], [11], and [12] require extensive model-based simulations that are time consuming and are topology-specific. The studies presented in [13], [14], [15], and [16] adopt an analytical approach with equivalent circuit modeling, which considers the switch node voltages as DM noise sources and then time-domain signals are converted to the frequency domain using fast Fourier transform (FFT). These approaches are not generalized and involve extensive mathematical computations. The authors in [17], [18], and [19] present a promising method for CrM topology for estimating DM noise by calculating the input current ripple harmonics using the Fourier analysis. This method has been demonstrated to be effective for single-phase boost PFC configurations; however, it is not applicable for more complex multileg multilevel topologies.

The currently available literature analyzes the input current ripple of a single-leg or two-leg interleaved CCM and CrM PFC converters, where the presented method of analysis and equations are valid only for the analyzed topology. Without a unified DM noise estimation approach, a different set of equations have to be extracted or simulations have to be performed to evaluate other TP PFC topology variants. Moreover, there is no existing literature that addresses multilevel TP PFC topology from the EMI point of view. These research gaps put a barrier for a fair comparison of passive component volumes among multileg and multilevel variants of TP PFC and make it difficult to identify the optimal number of legs and/or voltage levels, the operation mode, and the switching frequency of a TP PFC converter. In addition, it is challenging to decide which topology has higher power density for a specific application and power level. It is also difficult to compare CrM and CCM components in terms of passive volume without calculating the DM noise.

In this article, a unified analytical framework to estimate the DM noises for multileg and multilevel TP PFC converters by expressing the effective ripple current slopes in complex exponential form is proposed. With the proposed unified DM estimation method, the required DM filter for n-leg and l-level TP PFC variants can be found by sweeping the switching frequency. The outcome of the comparison of DM filter size serves as an important tool to choose the best switching frequency for each TP PFC topology considering system-level power density, and compare and identify the optimum TP PFC variant for a given specific target power. The preliminary work for this subject had been carried out in [20], where CCM and CrM TP PFCs are compared in terms of generated DM noise; however, the proposed DM noise estimation method has not been generalized for other TP PFC variants. In this article, a unified DM noise estimation method is applied to TP PFC variants shown in Fig. 1 and verified with the noise in the frequency spectrum obtained from the PSIM simulation environment followed by experiments. For a given inductance-switching frequency pair, the required noise attenuation is calculated, and the DM filters are designed for multileg and multilevel TP PFC converters. Next, the DM filter volume is empirically predicted and the boxed volumes of the DM filter for each topology are estimated based on the volume estimation approach provided in [21]. The total volume of the DM filter and the boost inductor is compared for different topologies at their best switching frequency operation points. The methodology presented in this article and the outcome of the comparison of DM filter size serve as an important tool to choose the best switching frequency for each TP PFC topology, which can be used to optimize converters for power density.

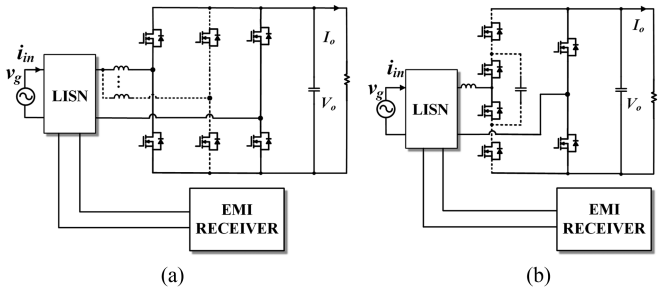

Fig. 1. TP PFC topologies. (a) Multileg variant. (b) Multilevel variant.

II. Unified DM Noise Estimation Method

A. DM Noise Estimation for CCM TP PFCs

The method to calculate the DM noise for multileg and multilevel TP PFC topologies is based on the Fourier analysis of the input current ripple. The complex Fourier coefficient for the input ripple current of single-leg CCM TP PFC is expressed as

$$c_{k,i_L}(d(t)) = \frac{V_o}{(2\pi^2\, k^2\, Lf_s)}\left(e^{-j2\pi k d(t)} - 1\right) \tag{1}$$

where k is the harmonic multiple of the switching frequency appearing in the EMI measurement band [17], i.e., ≥ 150 kHz. Note that (1) represents a time-varying complex harmonic function of input ripple current for a single-phase TP PFC. From (1), it can also be seen that it is a function of the duty cycle, which is expressed as in the following equation for CCM TP PFCs:

$$d(t) = 1 - \frac{\sqrt{2}V_g}{V_o}|\sin(\omega t)|. \tag{2}$$

After determining $c_{k,i_L}(d(t))$, an envelope detector is used to determine the generated DM noise. There are three types of detectors found in literature, namely "peak," "quasi-peak," and "average" envelope detectors. In this study, the average detector is considered; however, the method can be applied to other envelope detectors with ease. For a given harmonic multiple (k), the average ripple current value of kth harmonic can be determined by taking the average of (1) over the half-line cycle as

$$\langle c_{k,i_L}\rangle_{\text{avg}} = \frac{2}{T_g}\int_0^{\frac{T_g}{2}} c_{k,i_L}(d(t))dt \tag{3}$$

where T_g represents the period of the grid. The equivalent DM noise voltage in dB $\cdot\ \mu$ V is equal to the voltage drop across the resistance of the line impedance stabilization network (LISN) network, $R_{\text{LISN}} = 50\ \Omega$. The average of the complex harmonic function in the time domain corresponds to its magnitude in the frequency domain after taking its absolute value as given in

$$v_{\text{DM}}[\text{dB}\cdot\mu\text{V}] = 20\log\left(\frac{\left|\langle c_{k,i_L}\rangle_{\text{avg}}\right|\cdot R_{\text{LISN}}}{1\ \mu\text{V}}\right). \tag{4}$$

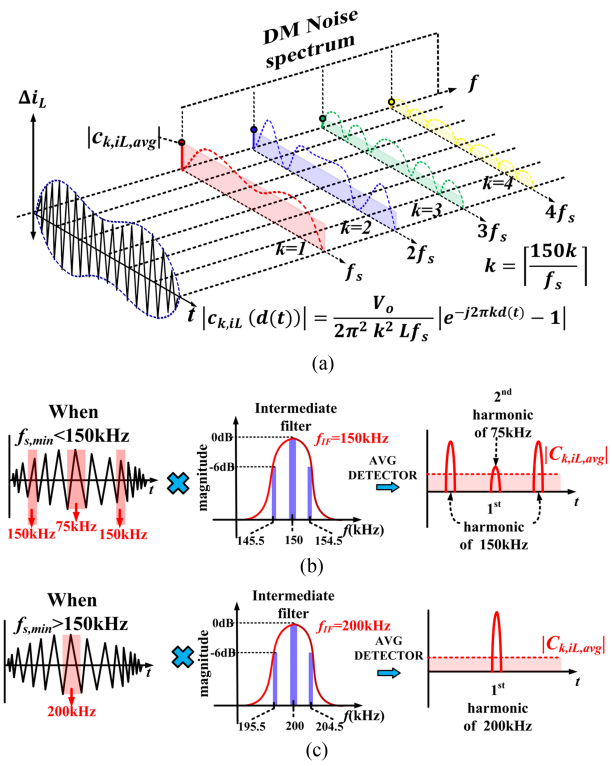

Fig. 2. DM noise estimation procedure illustration for (a) CCM TP PFCs, (b) CrM TP PFC for $f_{\text{s,min}}$ <150 kHz, and (c) CrM TP PFC for $f_{\text{s,min}}$ ≥150 kHz [20].

Fig. 2(a) illustrates the adopted approach for the calculation of DM noise in CCM TP PFCs, in which the complex harmonic function $c_{k,i_L}(d(t))$ is calculated using (1) for each kth harmonic and mapped into the frequency domain.

B. DM Noise Estimation for CrM TP PFCs

DM noise derivation for multileg CrM TP topology is not as straightforward as CCM TP topology as the switching frequency is variable resulting in distributed continuous harmonic spectrum of input ripple current instead of discrete harmonics multiples of f_s. Due to the time-varying switching frequency in the CrM converter, (1) is rewritten incorporating the time-dependent switching frequency as

$$c_{k,i_L}\left(f_s(t)\right) = \frac{V_o}{2\pi^2\, k^2\, L f_s(t)}\left(e^{-j2\pi k f_s(t) T_{on}} - 1\right). \quad (5)$$

The discrete frequency harmonic of interest can be extracted from the continuous spectrum using a Gaussian filter of particular bandwidth, centered at f_{IF}, as explained in [22], the Gaussian filter expression is given as

$$\left|G_{IF}\left(k, f_s(t)\right)\right| = e^{-\left(k f_s(t) - f_{IF}\right)^2 / \left(4.5\times 10^3/\sqrt{\ln(2)}\right)^2}. \quad (6)$$

Hence, ripple current harmonic at the desired frequency after filtration is given by

$$c_{k,i_L,\text{filter}}\left(f_s(t)\right) = c_{k,i_L}\left(f_s(t)\right)\cdot\left|G_{IF}\left(k, f_s(t)\right)\right|. \quad (7)$$

Afterward, one of the envelope detectors from "peak," "quasi-peak," and "average" is used to estimate the magnitude of the harmonic. For instance, the following envelope detectors are used to find peak and average values, respectively:

$$\left\langle c_{k,i_L,\text{filter}}\right\rangle_{\text{pk}} = \max\left(\sum_{k=1}^{N} c_{k,i_L,\text{filter}}\left(f_s(t)\right)\right) \quad (8)$$

$$\left\langle c_{k,i_L,\text{filter}}\right\rangle_{\text{avg}} = \text{mean}\left(\sum_{k=1}^{N} c_{k,i_L,\text{filter}}\left(f_s(t)\right)\right). \quad (9)$$

Here, $k = 1, 2, 3, \ldots, N$ and $N = \lceil f_{IF}/f_{s,\min}\rceil$. N represents the largest integer smaller than $f_{IF}/f_{s,\min}$, where f_{IF} = 150 kHz. The procedure to obtain the estimated DM noise at the desired frequency for CrM TP PFCs is illustrated in Fig. 2(b) and (c). As an example, two different cases are presented, in which the first one depicts when the minimum switching frequency of CrM mode is less than 150 kHz while in the other case, it is more than 150 kHz. The difference between the two cases is that subharmonics of noise at some other frequencies may contribute to the magnitude of DM noise at 150 kHz, when $f_{s,\min}$ < 150 kHz. For instance, when $f_{s,\min}$ = 75 kHz and the switching frequency variation is more than 75 kHz, the input current ripple contains the first harmonic of 150 kHz as well as the second harmonic of 75 kHz. Hence, the DM noise at f_{IF} = 150 kHz is contributed by 75 kHz (second harmonic) and 150 kHz (first harmonic). On the other hand, if $f_{s,\min}$ > 150 kHz, i.e., 200 kHz, $f_{IF} = f_{s,\min}$ and in this case, DM noise at f_{IF} is contributed only by 200-kHz component.

C. DM Noise Estimation for Multileg and Multilevel TP PFCs

The DM noise model mentioned above can be extended for multileg and multilevel TP PFCs as well. It is well known that DM noise is associated with the effective input current ripple; therefore, the Fourier analysis of the effective input current ripple for multileg and multilevel TP PFCs can be used to determine the DM noise. However, it's quite a cumbersome and time-consuming task to determine the expressions for effective input current ripple and then calculate the Fourier transform of them for each case. A much more efficient and easier way to find the generalized expression is to apply the effective slope determination approach along with obtaining the impulses associated with the effective input current ripple as discussed in this section.

1) Determination of Effective Slopes: For instance, in the case of three-leg interleaved TP PFC, there are three intervals in which the slope of the effective input current ripple is determined, as illustrated in Fig. 3. In the first interval when $0 < d \le 1/3$, the rising and falling slopes of input ripple are given as

$$m_{\text{in,rise}} = m_{\text{iL,rise}} - 2m_{\text{iL,fall}} \quad (10)$$

$$m_{\text{in,fall}} = -3m_{\text{iL,fall}}. \quad (11)$$

Similarly, when $1/3 < d \le 2/3$

$$m_{\text{in,rise}} = 2m_{\text{iL,rise}} - m_{\text{iL.fall}} \quad (12)$$

$$m_{\text{in.fall}} = m_{\text{iL.rise}} - 2m_{\text{iL.fall}} \quad (13)$$

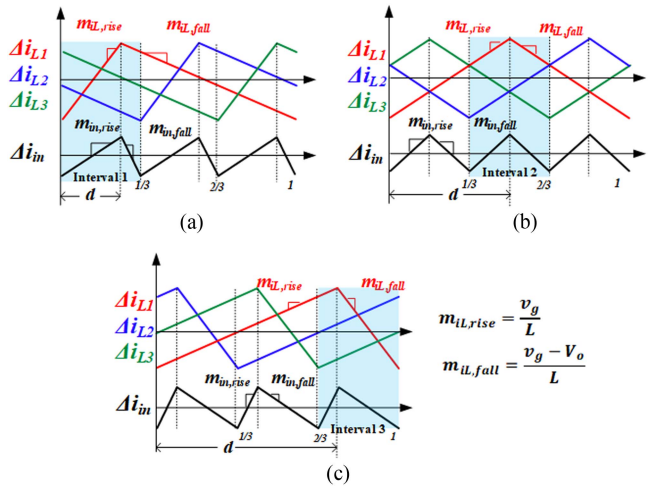

Fig. 3. Visualization of the slope of the effective input current ripple for three-leg interleaved case when (a) $0 < d \leq 1/3$, (b) $1/3 < d \leq 2/3$, and (c) $2/3 < d \leq 1$.

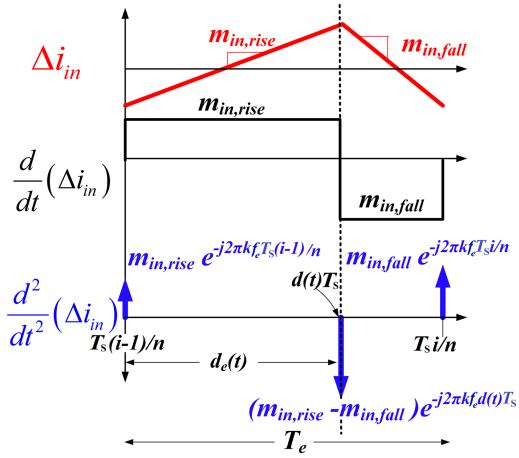

Fig. 4. Determination of the complex impulses from the slopes of the effective input current ripple in ith interval for n-phase interleaved case.

and when $2/3 < d \leq 1$

$$m_{\text{in,rise}} = 3m_{\text{iL,rise}} \tag{14}$$

$$m_{\text{in,fall}} = 2m_{\text{iL,rise}} - m_{\text{iL,fall}}\,. \tag{15}$$

Hence, the generalized expressions for the slopes of input current ripple based on the number of legs n and interval of duty cycle i for a given specific interval $(i-1)/n < d \leq i/n$ can be shown equal to

$$m_{\text{in,rise}} = i \cdot m_{\text{iL,rise}} - (n-i)m_{\text{iL,fall}} \tag{16}$$

$$m_{\text{in,fall}} = (i-1)m_{\text{iL,rise}} - (n-i+1)m_{\text{iL,fall}} \tag{17}$$

where $i = 1, 2, 3, \ldots, n$.

To determine the envelope of the effective current ripple harmonic for multileg interleaved TP PFCs, the generalized slopes are considered and impulses are determined as shown in Fig. 4. Any signal having finite-order time derivative in the form of scaled unit impulse functions, its Fourier series coefficients can be obtained by means of the Fourier expansion coefficients as explained in [23]. The complex envelope function for the effective current ripple harmonic is determined by adding all the impulses in the given effective time period T_{e}, and taking the double integration of the result to get back the expression for the effective input ripple current harmonic

$$\begin{aligned} c_{k,i}(d(t)) = \frac{2}{T_{\text{e}}}\frac{1}{(j2\pi k f_{\text{e}})^2}\Big(& m_{\text{in,rise}}\, e^{-j2\pi k f_{\text{e}}\frac{(i-1)}{n}T_{\text{s}}} \\ & - (m_{\text{in,rise}} - m_{\text{in,fall}})\, e^{-j2\pi k f_{\text{e}} d(t) T_{\text{s}}} \\ & + m_{\text{in.fall}}\, e^{-j2\pi k f_{\text{e}}\frac{i}{n}T_{\text{s}}}\Big)\,. \end{aligned} \tag{18}$$

Note that the above expression is for ith term at the effective switching frequency f_{e}, also the expression is in the complex domain, and the integration is achieved by multiplying it with $1/(j\omega k)$, where $\omega = 2\pi f_e$, $f_{\text{e}} = nf_{\text{s}}$, and k represents harmonic numbers. The final form of the generalized expression can be determined by adding all the terms as given in

$$\begin{aligned} & c_{k,n\phi}(d(t)) \\ & = \sum_{i=1}^{n}\left(c_{k,i}(d(t)) \quad \text{when } \frac{(i-1)}{n} < d(t) \leq \frac{i}{n}\right). \end{aligned} \tag{19}$$

2) Generalized Harmonic Function for N-Leg *Interleaving and* L-Level *Converter:* The relationship between the input current ripple of multileg interleaved and multilevel converters can be explained by comparing the two-leg interleaved and three-level (3L) TP PFC. The input current ripple expression for two-leg interleaved topology is derived as

$$\Delta i_{\text{in},2\phi}(t) = \begin{cases} \frac{1-2d(t)}{1-d(t)}\Delta i_{\text{L}}(t), & 0 < d(t) \leq \frac{1}{2} \\ \frac{2d(t)-1}{d(t)}\Delta i_{\text{L}}(t), & \frac{1}{2} < d(t) \leq 1 \end{cases}. \tag{20}$$

Similarly, the ripple current expression for 3L topology can be expressed as

$$\Delta i_{\text{in},3\text{L}}(t) = \frac{1}{2}\begin{cases} \frac{1-2d(t)}{1-d(t)}\Delta i_{\text{L}}(t), & 0 < d(t) \leq \frac{1}{2} \\ \frac{2d(t)-1}{d(t)}\Delta i_{\text{L}}(t), & \frac{1}{2} < d(t) \leq 1 \end{cases}. \tag{21}$$

Hence

$$\Delta i_{\text{in},1\phi,3\text{L}}(t) = \frac{1}{2}\Delta i_{\text{in},2\phi}(t). \tag{22}$$

Similarly, it can be easily proven mathematically that for an arbitrary n-leg, l-level TP PFC converter, the input current ripple is equal to a scaled-down version of the $[n \times (l-1)]$-leg TP PFC input current ripple. Here, the scaling factor is always $1/(l-1)$. The analytical proof involves extensive mathematical steps, so it has been omitted in this article. However, the simulation results for a 4-level, 2-leg TP PFC, and a 6-leg TP PFC are provided in Fig. 5 as a visual demonstration and serves as a proof of this concept. Therefore, the ripple current relationship between the *n-leg* interleaved and *l-level* topologies is derived as

$$\Delta i_{\text{in},n\phi,l\text{L}}(t) = \frac{1}{l-1}\Delta i_{\text{in},n(l-1)\phi}(t) \tag{23}$$

where l denotes the number of voltage levels. As the proposed method determines Fourier expansion coefficients from the input

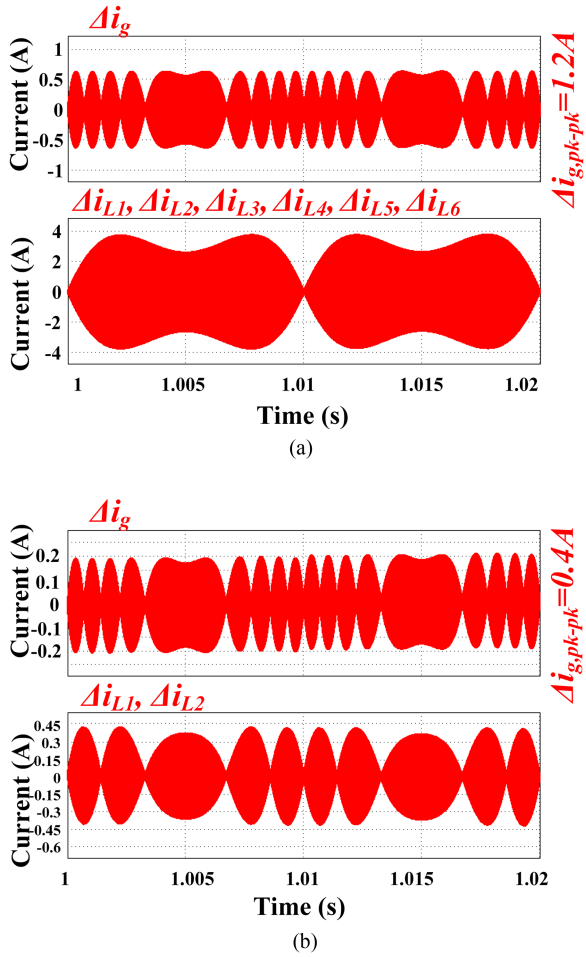

Fig. 5. Simulation waveform of input and inductor ripple currents for a line cycle of (a) 6-leg TP PFC and (b) 4-level 2-leg TP PFC.

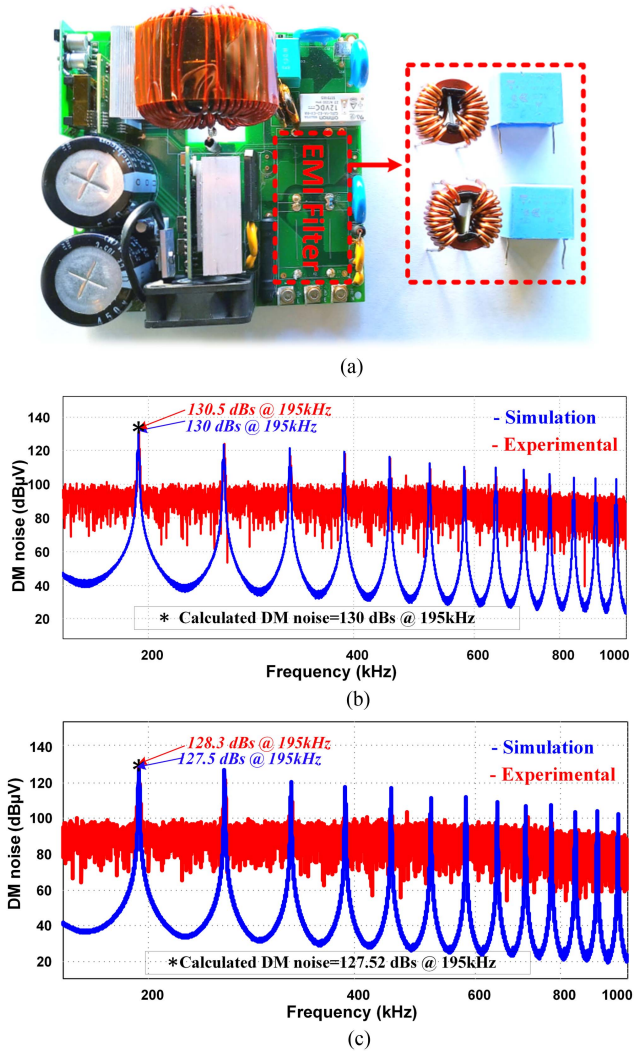

Fig. 6. Single-leg CCM TP PFC prototype switched at 65 kHz. (a) Photo of the prototype. (b) DM noise spectrum obtained from simulation, experiment, and calculation at $f_D = 195$ kHz for $V_g = 220$ $V_{\rm rms}$. (c) DM noise spectrum obtained from simulation, experiment, and calculation at $f_D = 195$ kHz for $V_g = 110$ $V_{\rm rms}$.

current ripple, any scaling on the input ripple current would directly affect the complex harmonic function that is composed of Fourier expansion coefficients. Hence, using (18), (19), and (23), the overall generalized expression of the complex harmonic envelope function for *n-leg*, *l-level* TP PFCs is found as

$$c_{k,n\phi,l\mathrm{L}}(d(t)) = \frac{2}{T_{\rm e}(l-1)}\frac{1}{(j2k\pi f_{\rm e})^2} \times \sum_{i=1}^{n'}\left[\begin{pmatrix} m_{\rm in,rise}e^{-j2\pi k f_{\rm e}\frac{(i-1)}{n'}T_{\rm s}} \\ -\left(m_{\rm in,rise}-m_{\rm in,fall}\right)e^{-j2\pi k f_{\rm e}d(t)T_{\rm s}} \\ +m_{\rm in,fall}e^{-j2\pi k f_{\rm e}\frac{i}{n'}T_{\rm s}}\end{pmatrix} \text{ when } \frac{(i-1)}{n'} < d(t) \le \frac{i}{n'}\right] \quad (24)$$

where $n' = n(l-1)$. In the CrM TP PFC case, $f_{\rm e}(t) = n'd(t)/T_{\rm on}$. When the power losses are assumed as zero, the turn-ON time in CRM TP PFC can be expressed as $T_{\rm on} = (2P_oL)/(nV_g^2)$. Once the input current ripple harmonic envelope functions are determined, the same steps can be followed as explained in the previous section to determine $v_{\rm DM}$ [dB μV] at desired switching frequency $f_{\rm D}$.

D. Validation of the Unified DM Noise Estimation Method

The proposed unified approach for estimating DM noise of multileg and multilevel CCM and CrM topologies is validated by comparing simulation results with that of experimental and calculated ones. For experimental validation purposes, the generated DM noises are measured on both single-leg CCM and 4L CCM TP PFC prototypes. Fig. 6(a) shows the test setup to carry out DM noise measurement for the single-leg TP PFC prototype running at 65 kHz with $L = 532$ μH at $V_o = 400$ V and under two different input voltages; 1) $V_g = 220$ $V_{\rm rms}$ and 2) $V_g = 110$ $V_{\rm rms}$. DM noise is measured without its EMI filter to get the actual DM noise by taking the FFT of the input current ripple. The experimental data are plotted along with the simulated and calculated results in Fig. 6(b) and (c). The calculated DM noise by the proposed estimation method is in close agreement with both the experimental and simulated results. It can be seen that the first harmonic appearing in the EMI spectrum ($\geq$150 kHz) is

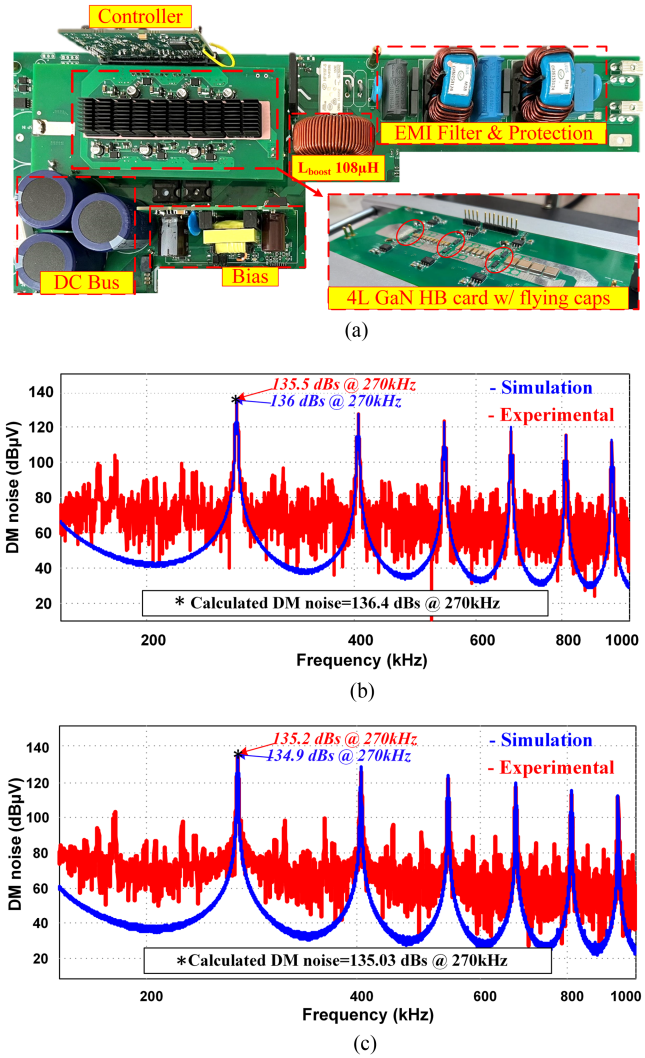

Fig. 7. DM noise measurement and estimation results. (a) Designed 4-Level CCM TP PFC prototype switched at 45 kHz. (b) Results of the simulation, experiment, and the calculated value at $f_D = 270$ kHz for $V_g = 220\ V_{\text{rms}}$. (c) Results of the simulation, experiment, and the calculated value at $f_D = 270$ kHz for $V_g = 110\ V_{\text{rms}}$.

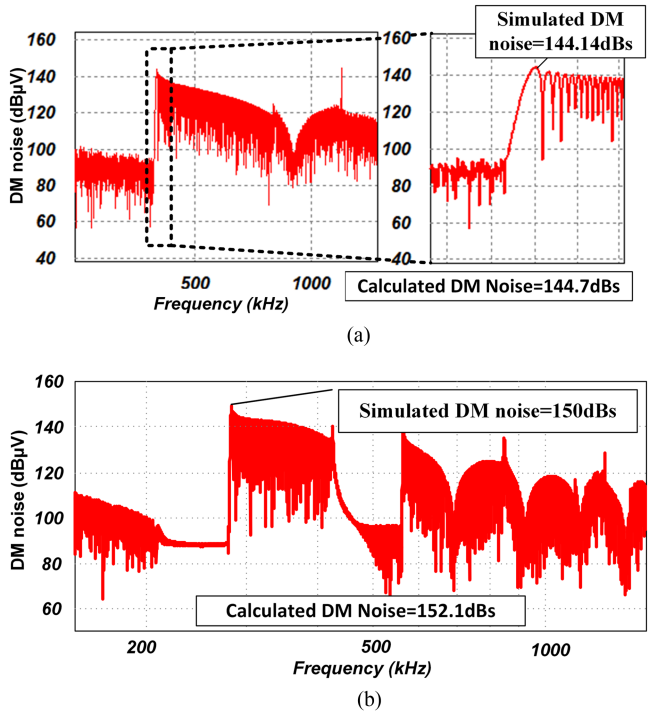

Fig. 8. DM noise simulation and estimation results for 2-leg CrM interleaved TP operated at $P_o = 3700$ W. (a) $V_g = 220\ V_{\text{rms}}$. (b) $V_g = 110\ V_{\text{rms}}$.

130 dB and 130.5 dB at 195 kHz in simulations and experiments, respectively for $V_g = 220\ V_{\text{rms}}$ case while the proposed method also calculates the noise as 130 dB at 195 kHz. Similarly, for the case of $V_g = 110\ V_{\text{rms}}$, the experimental DM noise is recorded as 128.3 dB, which is very close to the simulated (127.5 dB) and the calculated (127.52 dB) ones.

For the multilevel case, the DM noise has been measured on the designed 4-Level TP PFC prototype switched at 45 kHz with $L = 108\ \mu$H at $V_o = 380$ V under different input voltage, i.e., $V_g = 220\ V_{\text{rms}}$ and $V_g = 110\ V_{\text{rms}}$, as shown in Fig. 7(a). Similarly, the DM noise measurements are taken without the EMI filter for this prototype. The experimental data are plotted together with the simulated and calculated results for $V_g = 220\ V_{\text{rms}}$ and $V_g = 110\ V_{\text{rms}}$ as shown in Fig. 7(b) and (c), respectively. As can be seen from the figures, the obtained DM noise harmonic appearing in the EMI spectrum at 270 kHz is 136 dB for 220 V_{rms} and 134.9 dB for 110 V_{rms} in simulation, whereas it has been recorded as 135.5 dB for 220 V_{rms} and 135.2 dB for 110 V_{rms} experimentally. The proposed DM estimation method calculates the noise as 136.4 dB for 220 V_{rms} and 135.03 dB for 110 V_{rms}, which is within ± 1 dB of experimental and simulated results. More simulation results on other TP PFC variants can be found in [20].

To verify the proposed method on CrM TP PFC, a two-leg interleaved variant with $L = 14.25\ \mu$H at two different input voltages, i.e., 220 V_{rms} and 110 V_{rms} has been simulated, as shown in Fig. 8. The results in Fig. 8 show continuous spectra of DM noise because of the variable switching frequency operation of the topology. The results match with that of calculated ones with good precision making this method very useful in calculating the DM noise for the CrM case as well. The result for 3700 W and $V_g = 220\ V_{\text{rms}}$ shows that the peak of the DM noise within the EMI spectrum appears at 400 kHz, which is also the minimum input current ripple frequency. The simulation result for the DM noise at this frequency is observed as 144.14 dB, whereas the calculated value is 144.7 dB, as shown in Fig. 8(a). It can also be seen that a spike occurs at around 1.2 MHz, which is due to the DCM clamping of the converter to limit the maximum switching frequency. Similarly, the simulation result for $V_g = 110\ V_{\text{rms}}$ at $P_o = 3700$ W is provided in Fig. 8(b), in which the DM noise appears at 282 kHz with a magnitude of 150 dB, whereas it is calculated as 152.1 dB using the proposed estimation method.

III. Comparison of DM Filter Sizes Among n-Leg, l-Level TP PFCs Under CCM and Cr M Operations

After finding the DM noise voltage at the first harmonic appearing in the EMI measurement band, a DM filter providing

the required attenuation at the design frequency f_D is designed to meet the EMC standards. The method presented in [21] is used to find the boxed volumes of the DM filter inductors and capacitors. Designing the DM filter for converters with switching frequencies below 150 kHz requires further consideration as the switching frequency harmonics below 150 kHz may impact THD performance. Although the DM filter reduces the desired harmonic in the EMI measurement range, it may not provide enough attenuation at the switching frequency and its multiples below 150 kHz. Therefore, switching frequency harmonics below 150 kHz can also deteriorate THD to some extent if not mitigated with proper DM filter design. In the cases, where the DM filter does not provide significant attenuation around the switching frequency harmonic, the cutoff frequency of the first stage of the filter should be lowered to achieve sufficient attenuation at frequencies below 150 kHz. Conversely, the cutoff frequency of the second stage is increased. As a result, the size of the DM filter remains the same or may slightly increase in some cases. The DM filter size estimation given in this article only considers two identical filter stages.

A. DM Filter Size Comparison Among TP PFCs and Discussion

Since the DM noise is based on the current ripple envelope, the results of the comparison are highly dependent on the application power level, particularly for CrM TP PFC designs. On the other hand, the core of the input inductor is typically larger at higher power levels in CCM designs to avoid saturation, even if the inductance or the current ripple remains the same. In this section, filter sizes among different TP PFC variants are compared for the output power of 3700 W. The designers can compare filter sizes for different power levels by following the proposed framework.

1) CCM TP PFC Variants: For a fair comparison among different PFC variants, it is viable to keep the magnitude of the maximum effective input ripple current by selecting appropriate input inductances, even though the harmonic envelope will be different in each topology. For instance, when L is 400 μH for single-leg CCM TP PFC, the same ripple current amplitude is intuitively achieved in two-leg interleaved CCM TP PFC when L is 200 μH. Similarly, L=100 μH and L=50 μH provide the same ripple current amplitude for single-leg 3L and two-leg interleaved 3L variants, respectively. The comparison results for all the CCM topologies are provided in Fig. 9(a) and Table I.

In the case of single-leg CCM TP PFC, the minimum DM filter volumes are obtained at around f_s of 37, 45, 67, and 135 kHz considering the side-band harmonics. If f_s is increased slightly beyond 135 kHz, the DM filter volume is increased drastically as the fundamental harmonic and its side-band harmonics start to appear in the EMI measurement. Furthermore, it can be seen that f_s of 300 kHz results in a similar DM filter size. Therefore, choosing f_s in the range of 135 and 300 kHz does not bring any reduction in the DM filter size. It is worth noting that a single-stage DM filter becomes preferable when f_s is chosen more than 480 kHz.

The minimum DM filter volumes for two-leg interleaved and 3L topologies are achieved when f_s is equal to 67 kHz. In order to further lower the DM filter volume, f_s has to be pushed out more than 160 kHz, which is more challenging for hard-switched two-leg interleaved TP PFC as the FETs switch at full dc bus and experience greater switching losses compared to that of low-voltage FETs in the 3L converter. For higher power density, 3L TP PFC can be interleaved at the expense of increased cost. Fig. 9(a) also shows that the DM filter volume can be 108 cm^3 or even less at 88 kHz and beyond.

2) CrM TP PFC: The results of CrM TP PFC are a bit different in comparison to CCM TP PFCs, as there are no switching losses other than the circulating current losses, and the switching frequency is only limited by the core losses of the

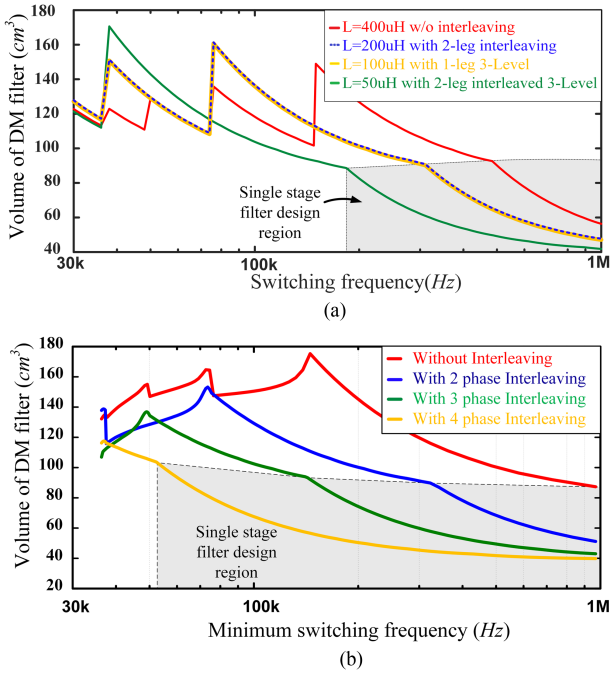

Fig. 9. DM filter volume comparison for (a) CCM variants over wide switching frequency range and (b) CrM variants over wide switching frequency range.

TABLE I
TOTAL DM FILTER VOLUMES AT CRITICAL FREQUENCIES FOR CCM TP PFCS

Topology	DM filter vol.(cm^3) at critical frequency f_s < 150 kHz				Min. DM filter vol. at f_s >150 kHz
	37 kHz	45 kHz	67 kHz	135 kHz	
1-leg CCM (400µH)	113	113	110	108	108 cm^3 at 300 kHz
2-leg CCM (200µH)	116	NC[1]	110	NC	110 cm^3 at 160 kHz
1-leg, 3L CCM (100µH)	116	NC	110	NC	110 cm^3 at 160 kHz
2-leg, 3L CCM (50µH)	113	NC	NC	NC	92 cm^3 at 151 kHz

[1]Noncritical frequency.

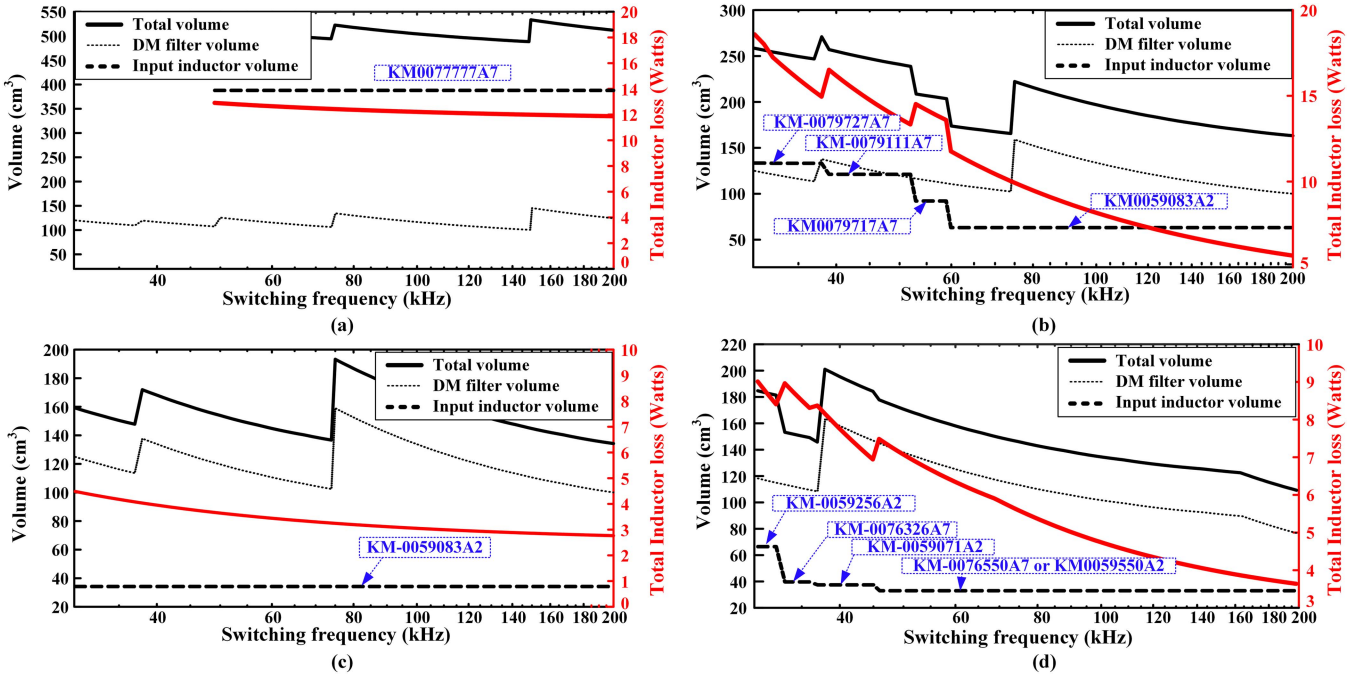

Fig. 10. DM filter size, input inductor volume, and input inductor losses versus frequency graph for (a) single-leg TP PFC, (b) interleaved TP PFC, (c) 3L TP PFC, and (d) 3L interleaved TP PFC.

input inductor. Fig. 9(b) suggests that the volume of the DM filter is significantly reduced as the number of the interleaving legs is increased due to the ripple cancellation effect and increase in the cutoff frequency of the DM filter. For a four-leg interleaved CrM at 3.7-kW output power, f_s of 46 kHz per leg results in a DM filter volume of 108 cm^3, whereas 300 kHz results in 45 cm^3, which is significantly lower than that of CCM cases.

B. DM Filter and Boost Inductor Volume Comparisons of CCM TP PFC Variants and CrM TP PFC

The DM filter size is highly dependent on the input inductance; thus, the volume of the boost inductor must be taken into account. The DM filter size, boost inductor volume, and inductor power loss variations with respect to switching frequency variations are shown in Fig. 10 for CCM TP PFC variants, where the inductors are designed using the framework presented in [24]. According to this, the inductor design is optimized based on volume and losses. It is seen from the figure that a lower switching frequency exhibits high inductor losses, and consequently requires bigger cores with high magnetic flux saturation. As the frequency is increased and the inductance is kept constant, the current ripple and the magnetic flux in the core are reduced. In the case of single-leg CCM TP PFC, kool-μ's KM-0077777A7(2-stacks), as shown in Fig. 10(a), is determined as the optimum core for the input inductor because other cores are either too small to accommodate the required number of turns or have too low B_{sat}. Note that there are no solutions for frequencies below 45 kHz as low f_s demands bigger cores than KM-0077777A7, which are not available in the used database.

The graph in Fig. 10(b) shows that the volume of the input inductor decreases with the increase in the frequency for a two-leg interleaved case. At the lowest frequency of interest, a bigger core KM-0079727A7 is selected as B_{sat} of the core satisfies the operating magnetic flux density, can accommodate the required number of turns within the allowed window area, and also gives low inductor loss. As the frequency is increased, even smaller cores are chosen that not only have smaller volumes but also lower losses. The loss curve in Fig. 10(b) depicts that the power losses slightly increase as the core shifts from bigger to smaller ones, mainly because the operating magnetic flux density increases due to the smaller cross-sectional area of the small volume core.

In Fig. 10(c), the volume and power loss curves of 3L single-leg CCM TP PFC are shown. In the f_s range of interest, the best inductor core is determined as KM-0059083A2, which has a significantly small volume, 34 cm^3. Therefore, the total volume trend follows the DM filter trend. The results show the clear advantage of 3L TP PFC over the two-leg interleaved TP PFC in terms of boost inductor size even though the generated DM noise levels are the same.

On the other hand, a 3L two-leg interleaved converter does not provide a significant advantage at low f_s as the inductors experience high core losses and require larger cores for cooling, as shown in Fig. 10(d). At higher f_s, the power losses decrease as both the ripple current and the magnetic flux density decrease. From 30 to 33 kHz, KM-0059256A2 is selected as the inductor core with a total volume of 66 cm^3, which is significantly higher than the 3L single-leg interleaved version. The total size of the inductors becomes equivalent to that of the 3L single-leg variant at f_s higher than 45 kHz.

The volume of the DM filter at critical frequencies for all the CCM TP PFC variants is between 108 cm^3 and 116 cm^3, which shows 5% variation. Hence, the DM filter volume is kept

TABLE II
DM FILTER AND BOOST INDUCTOR VOLUMES AT CRITICAL FREQUENCIES

Topology		Input inductance	f_s when DM filter volume $\approx$ 110cm^3 ±5%	Total inductor volume
CCM TP PFC	**Without interleaving**	400 µH	37 k/45 k/67 k/135 kHz	388 cm^3 @ 45 k/67 k/135 kHz
	2-leg interleaved	200 µH	37 k/67 kHz	68 cm^3 @ 67 kHz
3-Level CCM TP PFC	**Without interleaving**	100 µH	37 k/67 kHz	34 cm^3 @ 37 k/67 kHz
	2-leg interleaved	50 µH	37 k/88 kHz	33 cm^3 @ 88 kHz
CrM TP PFC	**2-leg interleaved**	16.17 µH	180 kHz (min frequency)	41 cm^3 @ 180 kHz losses=15.4+5.64 W core:3F3-E301507(2-stacks)
	3-leg interleaved	48.5 µH	90 kHz (min frequency)	58 cm^3 @ 90 kHz losses=11.66+7.56 W core:3F3-E301507(2-stacks)
	4-leg interleaved	126.5 µH	46 kHz (min frequency)	104 cm^3 @ 46 kHz losses=8.6+8.1 W core:3F3-E341409(2-stacks)

TABLE III
TOTAL DM FILTER AND BOOST INDUCTOR SIZE WHEN $f_s = 180$ kHz PER LEG IN CRM TP PFC

CrM TP PFC	L_{in}	Input inductance vol. at 180 kHz	DM filter vol.	Total Vol.
2-leg interleaved	16.17 µH	41 cm^3 (losses[a] 13.59 + 4.72W, 3F3-251311(2-stacks))	110 cm^3	151 cm^3
3-leg interleaved	24.2 µH	62 cm^3 (losses: 9.9 + 6.6W, 3F3-251311(2-stacks))	80 cm^3	142 cm^3
4-leg interleaved	32.4 µH	81 cm^3 (losses: 8.3 + 7.3W, 3F3-251311(2-stacks))	53 cm^3	134 cm^3

[a] Copper loss + Core loss.

fixed at 110 cm^3 with ±5% to make the comparison easy. All the feasible f_s and corresponding DM filter and input inductor volumes are obtained and provided in Table II. It must be noted that this minimum volume of 110 cm^3 is achieved at critical switching frequencies for 2L CCM TP without interleaving (i.e., 37 kHz, 45 kHz, 67 kHz, and 135 kHz) and with interleaving at 37 and 67 kHz. 3L CCM TP also achieves this volume at around the same critical frequencies. On the other hand, the interleaved 3L CCM TP achieves this volume at frequencies of 37 and 88 kHz. Since the DM filter size is similar at these frequencies, the minimum volume for the input inductor is obtained at the highest frequency among the given critical frequencies. In comparison to two-leg interleaved TP PFC, a 3L variant results in the smallest inductor with a volume of 34 cm^3. Even though a 3L 2-leg interleaved variant doubles the effective input ripple frequency and lowers the inductor size to 16.5 cm^3, the total inductor volume comes out to be 33 cm^3 as the interleaving structure uses two inductors instead of one. Therefore, the circuit complexity does not justify using this structure over a single-leg 3L converter.

To obtain 110 cm ^{3} of DM filter size in CrM TP PFC variants, the minimum switching frequencies along with corresponding input inductances are obtained at 180 kHz with 16.17 μH, 90 kHz with 48.5 μH, and 46 kHz with 126.5 μH, in case of 2-leg, 3-leg, and 4-leg interleaved CrM TP PFC topologies, respectively. The results summarized in Table II show that the volume of the input inductor may not necessarily decrease with the increase in the interleaving legs at low switching frequencies. This is due to the fact that a lower minimum switching frequency demands higher inductance, which results in a higher number of turns. Under this circumstance, the turns might not fit inside the small cores, despite the low flux density inside the core. To observe the advantage of multileg CrM TP PFCs, the converter must be designed for higher switching frequencies, where the input inductance requirement is small. To observe the effects, the minimum switching frequency of 180 kHz is kept the same among multileg structures, and DM filter size is analyzed as presented in Table III. With each interleaving leg, there is an additional inductor volume of 20.5 cm^3 contributing to the overall volume. Nevertheless, there is a significant reduction in the DM filter volume with the higher number of interleaving legs, which makes the total volume smaller. As seen from Table III, the total combined DM filter and boost inductor volumes are calculated as 151 cm^3 and 134 cm^3 for 2-leg and 4-leg interleaved CrM TP PFCs, respectively.

IV. CONCLUSION

This article proposed a unified analytical approach for the estimation of DM noise for both CCM and CrM multilevel and multileg TP PFC converters. The accuracy of the analytical method has been experimentally verified on both a 2-level single-leg CCM TP PFC with a 532-μH inductor switched at 65 kHz, and a 4-level single-leg CCM TP PFC with 108 μH switched at 45 kHz. The difference between the estimation and experimental results taken by the EMC receiver is less than 1 dB. The provided framework is used to estimate the DM noise and size of the DM filter by analyzing and calculating their boxed volumes for different TP variants over a wide switching frequency range.

Furthermore, DM filter and boost inductor volumes have been compared in an attempt the find the best switching frequency and total volume trend for each TP PFC variant. The results suggest that the minimum volume of DM filters for multileg and multilevel CCM TP PFC converters occurs at the critical

frequencies. For the same DM noise, the 3-level single-leg converter shows lower boost inductor volume in comparison to two-leg interleaved PFCs at the critical frequencies, meanwhile resulting in lower inductor losses. In order to improve the total volume further, either more legs need to be interleaved or the switching frequency needs to be increased over 270 kHz. The 3-Level 2-leg interleaved converter shows a decrease in the size of the converter at a relatively low frequency of around 88 kHz. On the other hand, it has been shown that CrM TP PFCs with a high number of interleaving legs show better performance at high switching frequencies. In case the switching frequency is limited for CrM TP PFCs, the two-leg interleaved CrM converter outperforms the higher number of interleaving leg CrM versions.

REFERENCES

[1] *Electromagnetic Compatibility (EMC) – Part 6 Generic Standards, Section 3: Emission Standard for Residential, Commercial and Light-Industrial Environments*, IEC 61000-6-3, International Electrotechnical Commission, Geneva, Switzerland, 2006.

[2] "Vehicles boats and internal combustion engines - radio disturbance characteristics - limits and methods of measurement for the protection of on-board receivers," Int. Special Committee Radio Interference (CISPR), Geneva, Switzerland, 2016.

[3] D. Shahzad, S. Pervaiz, N. A. Zaffar, and K. K. Afridi, "GaN-based high-power-density AC–DC–AC converter for single-phase transformerless online uninterruptible power supply," *IEEE Trans. Power Electron.*, vol. 36, no. 12, pp. 13968–13984, Dec. 2021.

[4] B. Whitaker et al., "A high-density, high-efficiency, isolated on-board vehicle battery charger utilizing silicon carbide power devices," *IEEE Trans. Power Electron.*, vol. 29, no. 5, pp. 2606–2617, May 2014.

[5] Q. Huang, R. Yu, Q. Ma, and A. Q. Huang, "Predictive ZVS control with improved ZVS time margin and limited variable frequency range for a 99% efficient, 130-W/in^3 MHz GaN totem-pole PFC rectifier," *IEEE Trans. Power Electron.*, vol. 34, no. 7, pp. 7079–7091, Jul. 2019.

[6] B. Sun, R. Burgos, and D. Boroyevich, "Common-mode EMI unterminated behavioral model of wide-bandgap-based power converters operating at high switching frequency," *IEEE J. Emerg. Sel. Topics Power Electron.*, vol. 7, no. 4, pp. 2561–2570, Dec. 2019.

[7] F. Luo, D. Boroyevich, P. Mattavelli, and X. Zhang, "On discussion of switching frequency impacts on DC-fed motor drive EMI filter design," in *Proc. IEEE 27th Annu. Appl. Power Electron. Conf. Expo.*, 2012, pp. 623–627.

[8] B. Sun, R. Burgos, and D. Boroyevich, "Assessment of switching frequency effect on a compact three-phase GaN-based inverter design," in *Proc. IEEE Energy Convers. Congr. Expo.*, 2018, pp. 868–875.

[9] A. C. Baisden, D. Boroyevich, and F. Wang, "Generalized terminal modeling of electromagnetic interference," *IEEE Trans. Ind. Appl.*, vol. 46, no. 5, pp. 2068–2079, Sep./Oct. 2010.

[10] W. Zhang, M. T. Zhang, F. C. Lee, J. Roudet, and E. Clavel, "Conducted EMI analysis of a boost PFC circuit," in *Proc. APEC 97- Appl. Power Electron. Conf.*, 1997, vol. 1, pp. 223–229.

[11] L. Yang et al., "Modeling and characterization of a 1 kW CCM PFC converter for conducted EMI prediction," in *Proc. IEEE 19th Annu. Appl. Power Electron. Conf. Expo.*, 2004, vol. 2, pp. 763–769.

[12] T. Nussbaumer, M. L. Heldwein, and J. W. Kolar, "Differential mode input filter design for a three-phase buck-type PWM rectifier based on modeling of the EMC test receiver," *IEEE Trans. Ind. Electron.*, vol. 53, no. 5, pp. 1649–1661, Oct. 2006.

[13] N. N. Esfetanaj, S. Peyghami, H. Wang, and P. Davari, "Analytical modeling of 9-150 kHz EMI in single-phase PFC converter," in *Proc. IEEE 45th Annu. Conf. Ind. Electron. Soc.*, 2019, vol. 1, pp. 4689–4693.

[14] N. N. Esfetanaj, H. Wang, F. Blaabjerg, and P. Davari, "Differential mode noise prediction and analysis in single-phase boost PFC for the new frequency range of 9-150 kHz," *IEEE J. Emerg. Sel. Topics Ind. Electron.*, vol. 3, no. 1, pp. 177–187, Jan. 2022.

[15] C. Wang, M. Xu, F. C. Lee, and B. Lu, "EMI study for the interleaved multi-channel PFC," in *Proc. IEEE Power Electron. Specialists Conf.*, 2007, pp. 1336–1342.

[16] N. N. Esfetanaj, H. Wang, F. Blaabjerg, and P. Davari, "Differential mode noise estimation and filter design for interleaved boost power factor correction converters," *Appl. Sci.*, vol. 11, no. 6, 2021, Art. no. 2716.

[17] Z. Wang, S. Wang, P. Kong, and F. C. Lee, "DM EMI noise analysis for critical conduction mode PFC," in *Proc. IEEE 26th Annu. Appl. Power Electron. Conf. Expo.*, 2011, pp. 1475–1481.

[18] Z. Wang, S. Wang, P. Kong, and F. C. Lee, "DM EMI noise prediction for constant on-time, critical mode power factor correction converters," *IEEE Trans. Power Electron.*, vol. 27, no. 7, pp. 3150–3157, Jul. 2012.

[19] F. Yang, X. Ruan, Q. Ji, and Z. Ye, "Input differential-mode EMI of CRM boost PFC converter," *IEEE Trans. Power Electron.*, vol. 28, no. 3, pp. 1177–1188, Mar. 2013.

[20] A. Tausif and S. Dusmez, "A differential mode noise estimation and filter size comparison in totem-pole PFC converters," in *Proc. IEEE PCIM Europe Digit. Days 2021; Int. Exhib. Conf. Power Electron.*, 2021, pp. 1–8.

[21] K. Raggl, T. Nussbaumer, and J. W. Kolar, "Guideline for a simplified differential-mode EMI filter design," *IEEE Trans. Ind. Electron.*, vol. 57, no. 3, pp. 1031–1040, Mar. 2010.

[22] T. Karaca, B. Deutschmann, and G. Winkler, "EMI-receiver simulation model with quasi-peak detector," in *Proc. IEEE Int. Symp. Electromagn. Compat.*, 2015, pp. 891–896.

[23] C. R. Paul, "Signal Spectra—the Relationship between the time domain and the frequency domain," *Introduction to Electromagnetic Compatibility*, 2nd ed. Hoboken, NJ, USA: Wiley, 2006, pp. 91–175.

[24] A. Lordoglu, M. O. Gulbahce, D. A. Kocabas, and S. Dusmez, "A new optimization method for gapped and distributed core magnetics in LLC converter," *IEEE Access*, vol. 11, pp. 14061–14072, 2023.

Ali Tausif (Student Member, IEEE) received the B.S. degree in electrical engineering from the College of Electrical and Mechanical Engineering, National University of Science and Technology, Islamabad, Pakistan, in 2014, and the master's degree in electrical engineering from the Department of Electric and Information Engineering, Seoul National University of Science and Technology, Seoul, South Korea, in 2019. He is currently working toward the Ph.D. degree in electrical engineering with Yildiz Technical University, Istanbul, Turkey.

In 2016, he joined the Power Electronics and Fuel Cell Power Conditioning Lab (PEFCL), SeoulTech, as a Graduate Research Student. His research interests include high-power-density converters for electric vehicle and renewable-energy systems.

Serkan Dusmez (Senior Member, IEEE) received the B.S. (Hons.) and M.S. degrees in electrical engineering from Yildiz Technical University, Istanbul, Turkey, in 2009 and 2011, respectively, the M.S. degree in electrical engineering from the Illinois Institute of Technology, Chicago, IL, USA, in 2013, and the Ph.D. degree in electrical engineering from The University of Texas at Dallas, Richardson, TX, USA, in 2016.

From 2016 to 2019, he was a System Engineer with Texas Instruments Incorporated, Dallas, TX, USA. Between 2019 and 2022, he was with Arcelik Global R&D serving as the Technical Leader. Since 2022, he has been a Technical Leader with WAT Motor A.S. He is the coauthor of more than 75 journal and conference papers and 7 US patents. His research interests include high power density solutions with GaN power stage and real-time fault diagnosis of power converters.

Dr. Dusmez is the recipient of the Marie Skäodowska-Curie Individual Fellowship awarded by the European Commission in 2021, and International Fellowship for Outstanding Researchers by the Scientific and Technological Research Council of Turkey in 2019. He is a recipient of the 2018–2019 IAS Second Prize Paper and 2017–2018 First Prize Paper both from the IEEE Industry Applications Society, the Jimmy Lin Award for Innovation from the University of Maryland at College Park in 2017, the First Prize Paper Award in the IEEE IAS Annual Meeting from the Industry Applications Society in 2016, and the 2015 Best Vehicular Electronics Paper Award from the IEEE Vehicular Technology Society.